Hindawi
Geofluids
Volume 2017, Article ID 2176932, 17 pages
https://doi.org/10.1155/2017/2176932

Review Article

A Review of Critical Conditions for the Onset of Nonlinear Fluid Flow in Rock Fractures

Liyuan Yu,[1] Richeng Liu,[1] and Yujing Jiang[2,3]

[1]*State Key Laboratory for Geomechanics and Deep Underground Engineering, China University of Mining and Technology, Xuzhou 221116, China*
[2]*State Key Laboratory of Mining Disaster Prevention and Control Co-Founded by Shandong Province and the Ministry of Science and Technology, Shandong University of Science and Technology, Qingdao 266590, China*
[3]*School of Engineering, Nagasaki University, Nagasaki 8528521, Japan*

Correspondence should be addressed to Richeng Liu; my1122002006@126.com

Received 9 April 2017; Accepted 9 May 2017; Published 6 July 2017

Academic Editor: Zhien Zhang

Selecting appropriate governing equations for fluid flow in fractured rock masses is of special importance for estimating the permeability of rock fracture networks. When the flow velocity is small, the flow is in the linear regime and obeys the cubic law, whereas when the flow velocity is large, the flow is in the nonlinear regime and should be simulated by solving the complex Navier-Stokes equations. The critical conditions such as critical Reynolds number and critical hydraulic gradient are commonly defined in the previous works to quantify the onset of nonlinear fluid flow. This study reviews the simplifications of governing equations from the Navier-Stokes equations, Stokes equation, and Reynold equation to the cubic law and reviews the evolutions of critical Reynolds number and critical hydraulic gradient for fluid flow in rock fractures and fracture networks, considering the influences of shear displacement, normal stress and/or confining pressure, fracture surface roughness, aperture, and number of intersections. This review provides a reference for the engineers and hydrogeologists especially the beginners to thoroughly understand the nonlinear flow regimes/mechanisms within complex fractured rock masses.

1. Introduction

Rock fracture network controls the main paths of fluid flow and contaminant migration in deep underground, and the estimation of permeability of fractured rock masses has been extensively studied during the past several decades in many geoengineering and geosciences such as CO_2 sequestration, enhanced oil recovery, and geothermal energy development [1–8]. The fluid flow in rock fractures and/or fracture networks is commonly assumed to obey the cubic law, in which the flow rate is linearly proportional to the pressure drop [9–13]. However, in the karst systems and/or in the vicinity of wells during pump tests, when the flow rate/velocity is large, fluid flow enters the nonlinear flow regime and flow rate is nonlinearly correlated with pressure drop [11, 14–16]. In such case, using the cubic law to calculate fluid flow will overestimate the conductivity of rock fractures and/or fracture networks [17–20]. Therefore, a thorough understanding of the nonlinear flow properties of fluid within fractures contributes to accurately predicting permeability of fractured rock masses [21].

Previous studies have reported that there are three representative types of nonlinear flow behaviors in rock fractures induced by inertial effect, fracture dilation, and solid-water interaction [16, 22, 23], and the present study focuses on the nonlinear flow behaviors induced by inertial effect. Many factors can affect the magnitude of permeability of fractured rock masses, including fracture length [24–27], aperture [28–30], surface roughness [31, 32], dead-end [33], number of intersections [34, 35], hydraulic gradient [36], boundary stress [37, 38], anisotropy [39–42], scale [43–46], stiffness [47], coupled thermo-hydro-mechanical-chemical (HTMC) processes [48–51], and precipitation-dissolution and biogeochemistry [52]. The discrete fracture network (DFN) model, which can consider most of the above parameters, has been increasingly utilized to simulate fluid flow in the complex

fractured rock masses [53–56], although it cannot model the aperture heterogeneity of each fracture [57–59]. In the numerical simulations and/or analytical analysis, the linear governing equation such as the cubic law is solved to simulate fluid flow in fractures by applying constant hydraulic gradients (J) on the two opposing boundaries, such as $J = 1$ [53, 60–64], $J = 0.1$ [37], $J = 0.001$ [65, 66], and J = unknown constants [10, 30, 42, 67–69]. This assumption that fluid flow obeys the cubic law is suitable for characterizing hydraulic behaviors of deep underground engineering, in which the flow rate is sufficiently small. For the fractured rock masses such as the karst system and/or the in situ hydraulic tests, the flow rate is relatively high and nonlinearly correlated with the pressure drop [14, 70]. With increasing pressure drop, the fracture network permeability decreases. To accurately simulate the nonlinear flow in fractures, the Navier-Stokes (NS) equations should be solved, which are composed of a set of coupled nonlinear partial derivatives of varying orders [17, 71, 72] and are more complex than solving the cubic law. When fluid flow is in the linear regime, each fracture in the two-dimensional DFNs is represented using a line segment [73], whereas when fluid flow enters the nonlinear regime and the NS equations are solved, the real geometry (void space) of each fracture that is formed with two walls should be incorporated, which to some extent increases the difficulty of establishing the models [36, 74]. As a result, both the yearly published papers and yearly cited times with the keywords "nonlinear flow" and "rock mass" are much smaller than those with the keywords "linear flow" and "rock mass," as shown in Figure 1. With the development of computing power, more researches are contributing to the nonlinear flow characteristics of fractures, which needs solving the NS equations and is often time-consuming. Therefore, it is a vital issue about how to determine the critical condition (i.e., critical Reynolds number or critical hydraulic gradient) for the onset of nonlinear flow.

This study firstly reviews the governing equations of fluid flow in fractures and then reviews the effects of shear displacement, normal stress and/or confining pressure, fracture surface roughness, fracture aperture, and fracture intersection on nonlinear flow characteristics of fractured rock masses. This work aims at providing a reference for engineers and researchers to quickly assess the magnitudes of critical Reynolds number or critical hydraulic gradient and to clearly understand the nonlinear flow mechanisms within complex fractured rock masses.

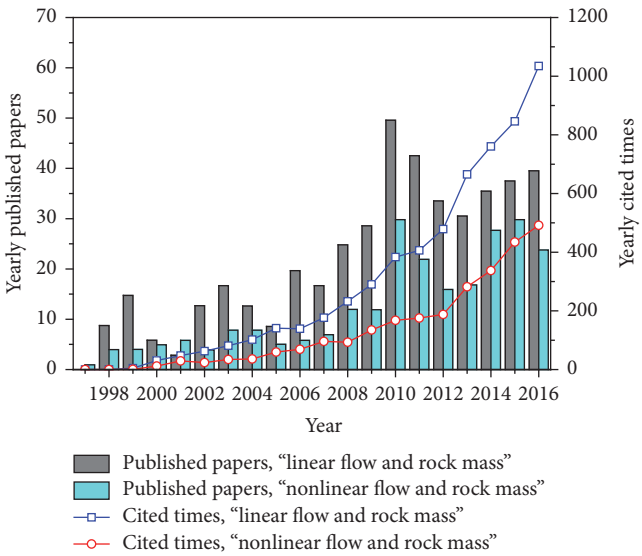

Figure 1: Yearly published papers and cited times with the keywords "linear flow and rock mass" and "nonlinear flow and rock mass." These data are collected from the Web of Science™ Core Collection (SCI-Expanded) over the past twenty years from 1997 to 2016.

2. Governing Equations of Fluid Flow in Fractures

2.1. Navier-Stokes Equations. The flow of incompressible Newtonian fluid is governed by the NS equations, written in a tensor form as [75–77]

$$\rho\left(\frac{\partial u_i}{\partial t} + u_i u_{i,j}\right) = \rho f_i - P_{,i} + \mu u_{i,jj}, \tag{1}$$

where u_i is the velocity of fluid in the i-direction in the Cartesian coordinate system with $i = x, y, z$ and $j = x, y, z$, respectively, the body force is $f_i = g_i = [0, 0, -g]$, ρ is the fluid density, t is the time, P is the pressure, and μ is the dynamic viscosity.

For steady-state flow, the parameters related to time t can be ignored and (1) gives

$$\rho u_i u_{i,j} = \rho f_i - P_{,i} + \mu u_{i,jj}. \tag{2}$$

Hydraulic head (h) is defined as the summation of elevation height (z_e) and hydraulic pressure head ($P/(\rho g)$), as follows:

$$h = z_e + \frac{P}{\rho g}. \tag{3}$$

Hydraulic gradient (J) is defined as the ratio of hydraulic head difference to flow length, written as

$$J_i = h_{,i} = \frac{1}{\rho g}\left(-\rho g_i + P_{,i}\right). \tag{4}$$

Substitution of (4) into (2) leads to a more abbreviated form of NS equations, as below [78]:

$$\rho u_i u_{i,j} = -\rho g h_{,i} + \mu u_{i,jj}. \tag{5}$$

2.2. Stokes Equations. When the flow rate/velocity is very small, which corresponds to a small Reynolds number (Re), the inertial term (the left term of (5)) can be negligible, resulting in the expression of the Stokes equations [79]:

$$h_{,i} = \frac{\mu}{\rho g} u_{i,jj}. \tag{6}$$

Equation (6) can be unfolded to the following forms:

$$h_{,x} = \frac{\mu}{\rho g}\left(u_{x,xx} + u_{x,yy} + u_{x,zz}\right),$$
$$h_{,y} = \frac{\mu}{\rho g}\left(u_{y,xx} + u_{y,yy} + u_{y,zz}\right), \quad (7)$$
$$h_{,z} = \frac{\mu}{\rho g}\left(u_{z,xx} + u_{z,yy} + u_{z,zz}\right).$$

2.3. Reynolds Equation. Dimensional analysis is performed and some definitions are made: Λ is the dimension of fracture in xy-plane, U is the dimension of flow velocity in both x- and y-directions, V is the dimension of flow velocity in z-direction, and a is the dimension of fracture aperture.

$$\begin{aligned}
&\mathrm{mag}\left[\frac{\partial^2 u_x}{\partial x^2}\right] \approx \mathrm{mag}\left[\frac{\partial^2 u_x}{\partial y^2}\right] \approx \frac{U}{\Lambda^2},\\
&\mathrm{mag}\left[\frac{\partial^2 u_x}{\partial z^2}\right] \approx \frac{U}{a^2},\\
&\mathrm{mag}\left[\frac{\partial^2 u_y}{\partial x^2}\right] \approx \mathrm{mag}\left[\frac{\partial^2 u_y}{\partial y^2}\right] \approx \frac{U}{\Lambda^2},\\
&\mathrm{mag}\left[\frac{\partial^2 u_y}{\partial z^2}\right] \approx \frac{U}{a^2},\\
&\mathrm{mag}\left[\frac{\partial^2 u_z}{\partial x^2}\right] \approx \mathrm{mag}\left[\frac{\partial^2 u_z}{\partial y^2}\right] \approx \frac{U}{\Lambda^2},\\
&\mathrm{mag}\left[\frac{\partial^2 u_z}{\partial z^2}\right] \approx \frac{U}{a^2}.
\end{aligned} \quad (8)$$

When the dimension of fracture aperture is much less than the dimension of fracture in the xy-plane ($a \ll \Lambda$), in which case the tortuosity of fracture void space is very small, the first two terms of (8) is much less than the last term and can be negligible. As a result, (7) can be simplified to the following equations:

$$h_{,x} = \frac{\mu}{\rho g} u_{x,zz}, \quad (9)$$

$$h_{,y} = \frac{\mu}{\rho g} u_{y,zz}, \quad (10)$$

$$h_{,z} = \frac{\mu}{\rho g} u_{z,zz}. \quad (11)$$

When the fracture aperture and the change in hydraulic head in the z-direction are small, (11) yields

$$h_{,z} \approx 0. \quad (12)$$

Substitution of (12) into (9)~(11) gives

$$\begin{aligned}
u_x(x,y,z) &= \frac{\rho g}{2\mu}\left(h_{,x}\right)\left(z^2 + b_1 z + c_1\right),\\
u_y(x,y,z) &= \frac{\rho g}{2\mu}\left(h_{,y}\right)\left(z^2 + b_2 z + c_2\right),\\
h &= h(x,y),
\end{aligned} \quad (13)$$

where b_1, b_2, c_1, and c_2 are the integration constants.

Importing non-slip boundary conditions results in

$$\begin{aligned}
u_x &= 0,\\
u_y &= 0,\\
&\text{when } z = \pm\frac{E}{2},
\end{aligned} \quad (14)$$

where E is the fracture aperture, and $z = \pm E/2$ are the lower and upper bounds of fracture void space in the z-direction.

Substitution of (14) into (13) leads to the values of integration constants (b_1, b_2, c_1, and c_2), and (13) can be rewritten as

$$u_x(x,y,z) = \frac{\rho g}{2\mu}\left(h_{,x}\right)\left(z + \frac{E}{2}\right)\left(z - \frac{E}{2}\right), \quad (15)$$

$$u_y(x,y,z) = \frac{\rho g}{2\mu}\left(h_{,y}\right)\left(z + \frac{E}{2}\right)\left(z - \frac{E}{2}\right), \quad (16)$$

$$h = h(x,y). \quad (17)$$

Integrations of (15) and (16) along the z-direction leads to

$$\begin{aligned}
q_x &= \int_{-E/2}^{E/2} u_x\, dz = -\frac{\rho g E^3}{12\mu}\frac{\partial h}{\partial x},\\
q_y &= \int_{-E/2}^{E/2} u_y\, dz = -\frac{\rho g E^3}{12\mu}\frac{\partial h}{\partial y},
\end{aligned} \quad (18)$$

where q_x is the flow rate in the x-direction, and q_y is the flow rate in the y-direction.

The law of conservation of mass of flow rate is expressed as [80]

$$q_{x,x} + q_{y,y} = 0. \quad (19)$$

Thus, substituting (18) into (19) results in the Reynolds equation, given as [17]

$$\frac{\partial}{\partial x}\left(\frac{\rho g E^3}{12\mu}\frac{\partial h}{\partial x}\right) + \frac{\partial}{\partial y}\left(\frac{\rho g E^3}{12\mu}\frac{\partial h}{\partial y}\right) = 0. \quad (20)$$

2.4. Cubic Law. An assumption is made that fluid flows through two infinite smooth parallel plates with a constant aperture E, as shown in Figure 2. Because fluid flows along the x-coordinate, the flow velocities in the y- and z-directions equal zero.

$$u_y = u_z = 0. \quad (21)$$

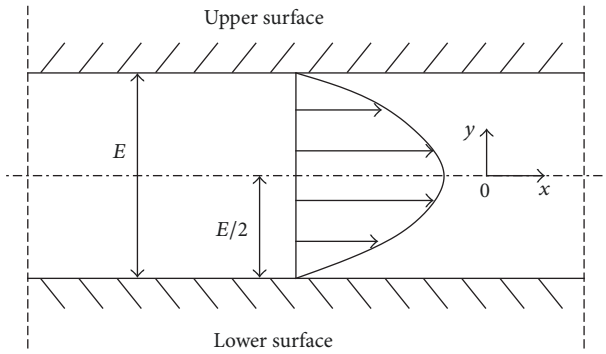

Figure 2: Flow velocity distribution in a parallel plate model.

The continuity equation of fluid is

$$\frac{\partial \rho}{\partial t} + \left(\rho u_i\right)_{,i} = 0. \tag{22}$$

For incompressible fluid, (22) can be simplified to

$$u_{i,i} = 0. \tag{23}$$

Substitution of (21) into (5) gives the governing equation of fluid flow in the x-direction, written as

$$\rho u_x u_{x,x} = -\rho g h_{,x} + \mu u_{x,xx}. \tag{24}$$

Substituting (23) into (24) gives rise to the fact that the left term equals zero.

$$0 = -\rho g h_{,x} + \mu u_{x,xx}. \tag{25}$$

Importing the non-slip boundary conditions (see (14)) and integrating (25) lead to

$$Q = \int_{-E/2}^{E/2} u_x \, dz = -\frac{E^3}{12\mu}\frac{\partial P}{\partial x}, \tag{26}$$

where Q is the flow rate through a fracture.

Equation (26) is the expression for the cubic law, in which fracture width (w) is assigned a constant value of 1. When $w \neq 1$, w should be introduced in (26), as follows:

$$Q = -\frac{wE^3}{12\mu}\frac{\partial P}{\partial x}. \tag{27}$$

2.5. Forchheimer Equation. With increasing flow velocity or Re, the flow rate is nonlinearly correlated with pressure drop and (27) is no longer applicable. Some empirical expressions were proposed to describe this nonlinear relationship, among which the Forchheimer equation is widely used where the pressure drop is a quadratic function of flow rate, expressed as [82–87]

$$-\nabla P = AQ + BQ^2, \tag{28}$$

where A and B are two coefficients that represent the linear and nonlinear terms of fluid flow, respectively. When Q is very small, the nonlinear term (BQ^2) can be negligible and drops out. In this case, (28) reduces to

$$-\nabla P = AQ, \tag{29}$$

where A is a constant that equals $12\mu/wE^3$ if the fracture is not deformable. Equation (28) can probably be applied over the entire range of flow rate/velocity, including that it reduces to linear Darcy's law (29) at a sufficiently low flow rate/velocity. Another macroscopic nonlinear flow equation to characterize the nonlinear flow in rock fractures is Izbash's law (Izbash 1931), but it cannot well quantify the linear flow properties at a sufficiently low Re. Therefore, the two equations can both be utilized to describe the nonlinear relationships between flow rate and pressure drop, especially for strong inertial regime; however, only the Forchheimer equation is used to depict the critical Reynolds number by directly plotting the normalized transmissivity–Reynolds number curves [88–90].

To describe the nonlinearity of fluid flow, a nonlinear factor (N_f) is defined as

$$N_f = \frac{BQ^2}{AQ + BQ^2}. \tag{30}$$

N_f denotes the ratio of pressure drop caused by the nonlinear term (BQ^2). In the previous works, it is assumed that the critical Reynolds number (Re_c) is the Re that corresponds to $N_f = 0.1$ [88, 91–93].

Besides the dimensionless Re that is used for characterizing the transition from linear to nonlinear flow regimes, the dimensionless Forchheimer number (F_0) is another widely accepted parameter, which is defined as the ratio of nonlinear to linear pressure losses, written as [16, 90, 94]

$$F_0 = \frac{BQ^2}{AQ} = \frac{BQ}{A}. \tag{31}$$

Thus, (30) can be rewritten as

$$N_f = \frac{F_0}{1 + F_0}. \tag{32}$$

The transmissivity (T), which is a commonly used parameter to describe the conductivity of a fracture, is defined as

$$T = \frac{E^3}{12} = -\frac{\mu Q}{w\nabla P}. \tag{33}$$

When fluid flow is in the linear regime, T is a constant and is represented using T_0. Thus the ratio of T to T_0 can be calculated according to

$$\frac{T}{T_0} = \frac{-\mu Q/w\left(AQ + BQ^2\right)}{-\mu Q/w\left(AQ\right)} = \frac{AQ}{AQ + BQ^2} = 1 - N_f. \tag{34}$$

Therefore, $T/T_0 = 0.9$ and $N_f = 0.1$ have the same physical meaning that the nonlinear term (BQ^2) contributes to 10% of the pressure drop, in which the current Re is Re_c.

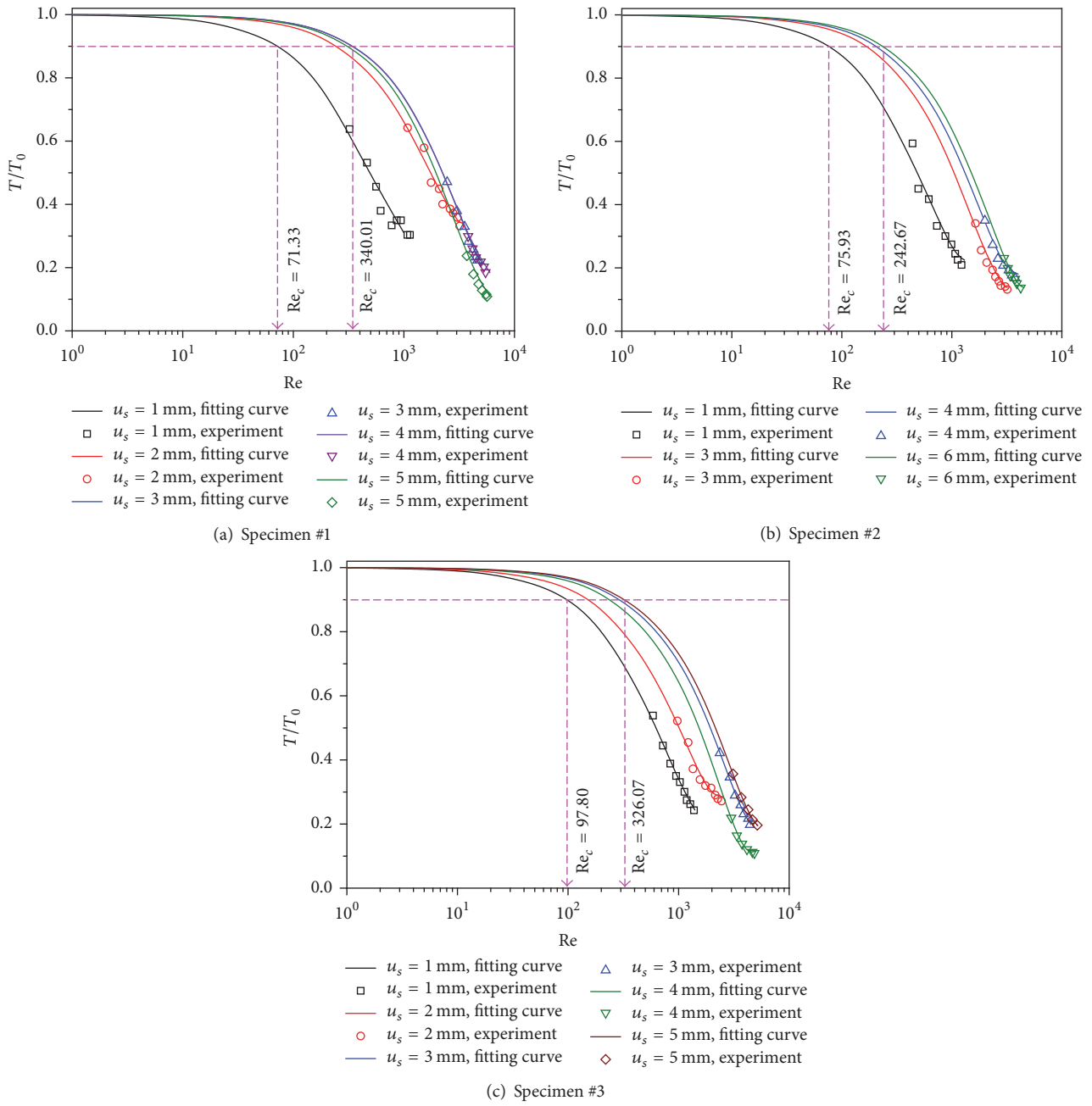

FIGURE 3: Relationships between T/T_0 and Re based on the data replotted from Xia et al. ([81], Figure 10).

3. Nonlinear Flow Characteristics of Rock Fractures

3.1. Effect of Shear Displacement. Under a constant normal stress, increasing shear displacement (u_s) can change the void space of a fracture. As a result, both the average aperture and permeability/transmissivity increase by up to 3 orders of magnitude with a maximum of u_s of 16 mm [95–99]. This variation of fracture void space during shear can also change the nonlinear flow properties of fluid such as the critical Reynolds number Re_c, which is used for characterizing the onset of nonlinear flow. Xia et al. [81] conducted laboratory experiments on three artificial rock joints having natural joint surface characteristics to investigate the nonlinear flow behaviors under different shear displacements. The cylindrical specimens that were cored from marble blocks taken from the construction site of Jin-Ping-II Hydropower Station in China have a diameter of 50 mm and a length of 100 mm. The average values of joint roughness coefficient (JRC) of the three samples are 13.28, 15.09, and 11.23, respectively. By fitting their results, it is found that when Re is small (i.e., less than 10), with the increment of Re, T/T_0 holds approximately constant value of 1 (see Figure 3). With continuously increasing Re, T/T_0 decreases. When $T/T_0 = 0.9$, Re_c is calculated,

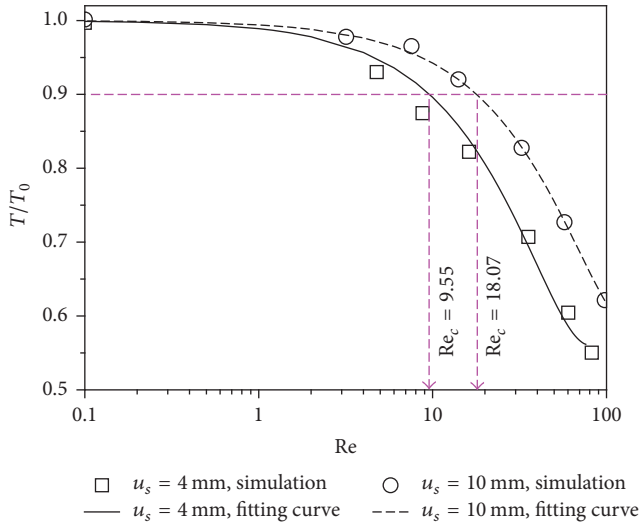

FIGURE 4: Relationships between T/T_0 and Re based on the data replotted from Xiong et al. ([95], Figure 12(a)).

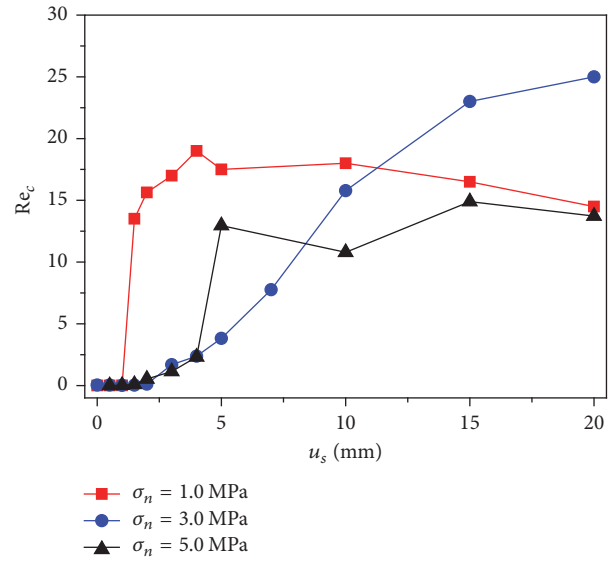

FIGURE 5: Relationships between Re_c and u_s based on the data replotted from Javadi et al. ([90], Figure 8).

which is in the ranges 71.33~340.01 (u_s = 1~5 mm), 75.93~242.67 (u_s = 1~6 mm), and 97.80~326.07 (u_s = 1~5 mm), respectively. The range of Re_c (from 71.33 to 340.01) is much less than that (from 1408.2 to 5674.4) calculated in the original works, because they used T/T_0 = 0.1 to quantify the onset of nonlinear flow, in which the nonlinear term contributes to 90% of the pressure drop. They also reported that, with increasing u_s, both the linear and nonlinear coefficients (A and B) in Forchheimer equation decrease. Xiong et al. [95] simulated the coupled shear-flow behaviors by directly solving the NS equations using the geometries of two natural rock fractures labelled with J3 and J7, whose JRC equals 17~18 and 3~4, respectively. The relationships between T/T_0 and Re as shown in Figure 4 exhibit the same variation trend with those in Figure 3. With increasing u_s from 4 mm to 10 mm, Re_c increases from 9.55 to 18.07, because the larger u_s gives rise to the larger fracture aperture and a smaller number of contacts, which results in the increment of Re_c. Javadi et al. [90] experimentally investigated the role of shear processes on Re_c for nonlinear flow through rough-walled fractures. The normal stress (σ_n) ranges from 1.0 to 5.0 MPa and u_s = 0~20 mm. The results show that when u_s = 0~1 mm, Re_c has very small values approaching 0 for all cases (see Figure 5). When u_s = 1~5 mm, Re_c dramatically increases for σ_n = 1.0 MPa and 5.0 MPa but gently increases for σ_n = 3.0 MPa. For u_s = 5~20 mm, the Re_c holds approximately constant values for σ_n = 5.0 MPa and slightly decreases for σ_n = 1.0 MPa; however the Re_c continuously increases for σ_n = 3.0 MPa. The different variations of $Re_c \sim u_s$ curves may be induced by the statistical distributions of void space of fractures during shear. The range of Re_c is from 0.001 to 25. Rong et al. [100] prepared 6 granite fractures with JRC = 6.67~8.18 and conducted coupled shear-flow tests with σ_n = 0.5~3.0 MPa and u_s = 0.0~10.9 mm. The results shown in Figure 6 depict that when u_s = 0~0.5 mm, with the increment of u_s, Re_c decreases, which is very different from those presented in Figure 5. With increasing u_s from 0.5 to 3.0 mm, Re_c increases dramatically and then varies negligibly small when u_s exceeds 3.0 mm. This variation trend is similar to that (with σ_n = 1.0 or 5.0 MPa) reported in Javadi et al. [90]. As an example, when σ_n = 1.0 MPa, Re_c that corresponds to a small u_s in the work of Javadi et al. [90] is much smaller than that in the work of Rong et al. [100]; however when u_s is relatively large, Re_c in the work of Javadi et al. [90] is approximately 2.0~2.5 times that in the work of Rong et al. [100]. The differences of Re_c evolution are dependent on fracture's morphology such as mean JRC. Zimmerman et al. [88] presented a high-resolution NS simulation and laboratory measurements of fluid flow in a natural sandstone fracture. The two opposing fracture surfaces were made using epoxy casts [101, 102], which has a size of 2 cm × 2 cm. By fitting the tested and computed results, Figure 7 depicts that Re_c equals 12.56 for the experiment and 21.92 for the simulation, which is near the range of Re_c reported in literature [90, 95].

3.2. Effects of Normal Stress and/or Confining Pressure. The normal stress applied on a cuboid sample and/or confining pressure applied on a cylindrical sample can decrease the permeability of rock mass, following exponential functions [103–108]. With increasing the normal stress σ_n, both the fracture closure u_n and the increasing rate increase as shown in Figure 8, where $u_{n\max}$ is the maximum closure and k_{n0} is the initial stiffness [109, 110]. This aperture variation/closure caused by normal stress contributes to the magnitudes of Re_c and/or J_c. Zhang and Nemcik [111] studied the fluid flow regimes and nonlinear flow characteristics in deformable rock fractures through flow tests on four cylindrical grain sandstone samples under confining stresses from 1.0 MPa to 3.5 MPa. They analyzed the variations of nonlinear factor B describing flow in deformable rock fractures and reported that the confining stress does not change both the linear and nonlinear flow patterns but has a significant influence on flow characteristics.

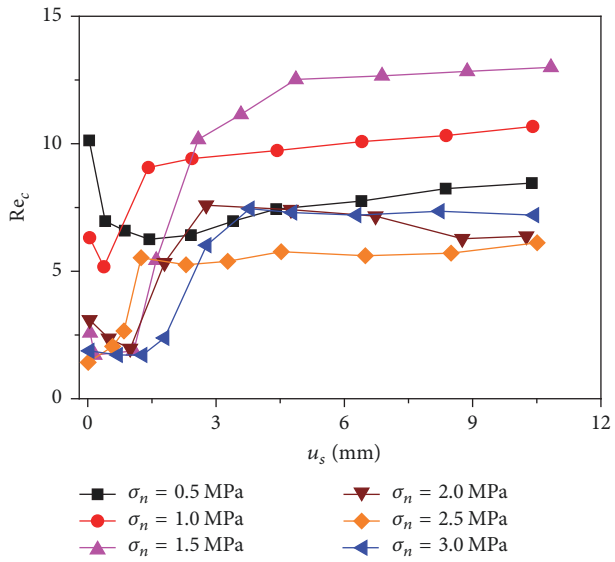

FIGURE 6: Relationships between Re_c and u_s based on the data replotted from Rong et al. ([100], Figure 9).

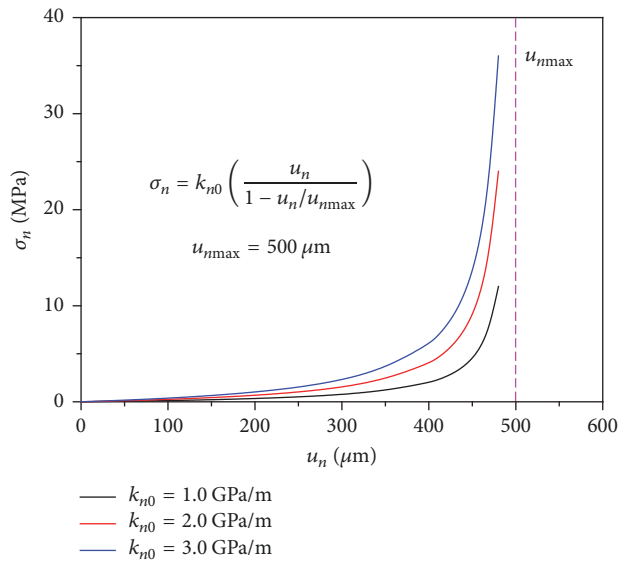

FIGURE 8: Relationships between σ_n and u_n with different k_{n0}.

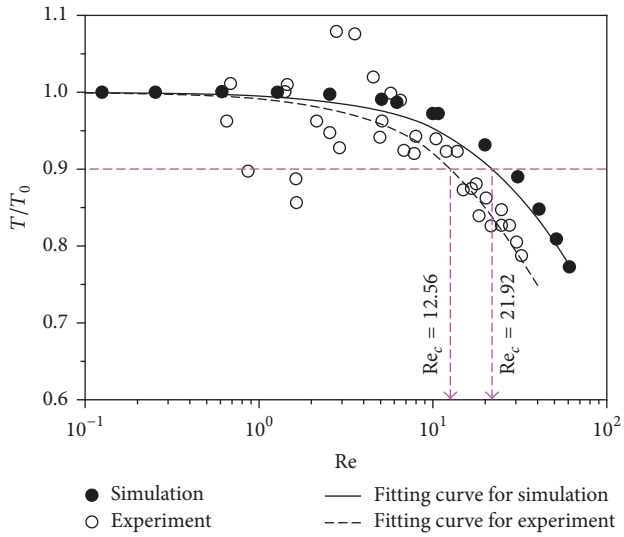

FIGURE 7: Relationships between T/T_0 and Re based on the data replotted from Zimmerman et al. ([88], Figure 2).

With increasing JRC from 5.5 to 15.4, the range of Re_c under different confining stresses is 21.96~40.34, 46.73~66.84, 40.35~51.70, and 26.13~32.38, respectively, as shown in Figure 9. The calculated ranges of Re_c are several times larger than those calculated by Zhang and Nemcik [111], in which the corresponding Re_c = 3.5~4.5, 13.1~17.6, 19.3~24.8, and 6.3~8.6, respectively. The potential reason may be that, in the study of Zhang and Nemcik [111], the flow has entered the strong nonlinear regimes, where the factor A calculated using the fitted Forchheimer equation cannot be accurately estimated. That means, in such a situation, changing the magnitude of A will have negligible effect on the correlation coefficient between the tested results and fitted curves of Forchheimer equation, but it can robustly change the variations of N_f, resulting in the smaller ranges of Re_c. This is the reason why we would like to use the variations of T/T_0 rather than N_f in the present study. Ranjith and Darlington [89] conducted nonlinear single-phase flow tests on real cylindrical rock joints with 110 mm height and 55 mm diameter under different confining pressures. The results depicted that, with increasing σ_n from 1.0 MPa to 5.0 MPa, Re_c decreases from 31.29 to 28.77 (see Figure 10), which is in a smaller range compared with those in Figure 9. Chen et al. [112] presented the high-pressure packer test (HPPT) observations performed in fractured rock masses, which is located at about 450 m in depth in Qiongzhong County, China. Four test boreholes numbered ZK124, ZK126, ZK129-1, and ZK129-2, respectively, were obtained from in situ cites in the depths ranging from 33.4 m to 142.1 m with numbers of test intervals from 6 to 16, and the flow rate-pressure drop relationships as well as the magnitude of Re_c were calculated. By collecting the tested results and replotting them in Figure 11, the variations of Re_c with depth show that, for all boreholes, Re_c fluctuates significantly in the range 25~66 and does not exhibit strong relationships with depth. The reasons may be that the boreholes at different depths contain fractures having different geometric properties such as aperture, persistence, orientation, and surface roughness. To simplify the model and clearly investigate the influence of normal stress and/or confining pressure on Re_c, Zhou et al. [94] prepared four granite rock samples (G1~G4) taken from the depth 450~550 m in the Beishan area in Gansu Province, China, and two sandstone rock samples (S1~S2) taken from the depth of about 20 m in the Three Gorges Reservoir area, Hubei Province, China. The confining pressure varies from 1.0 to 30.0 MPa and Re_c under each confining pressure is calculated. The results depicted in Figure 12 show that, with increasing confining pressure, Re_c firstly increases and then decreases for the samples G2~G4 and S1~S2, because when the confining pressure is small, the decreased aperture due to the elastic

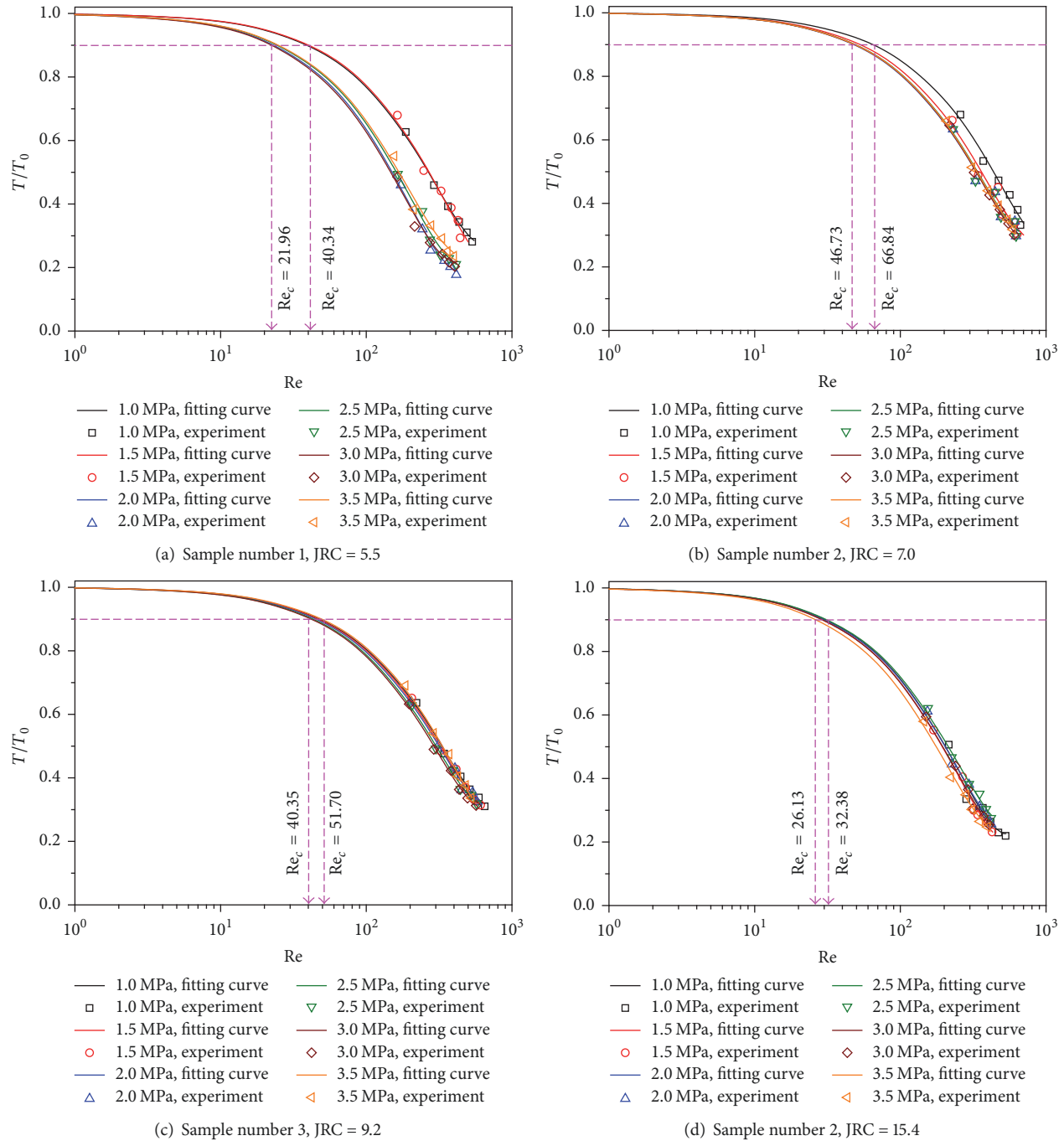

FIGURE 9: Relationships between T/T_0 and Re based on the data replotted from Zhang and Nemcik ([111], Figure 8).

compression will increase Re_c [36]. When continuously increasing confining pressure, the contacts between two fracture walls are destroyed and the microfractures may propagate within rocks and the split rock fragments will be clamped by the two walls, which gives rise to complex flow behaviors and decreases Re_c. For the sample G1, with increasing confining pressure, Re_c steadily decreases and shows a different variation trend with other samples. They reported that Re_c for the samples G1~G4 and S1~S2 varies in the ranges 0.075~9.243, 0.120~4.467, 0.160~5.108, 0.039~4.509, 0.191~4.090, and 0.026~2.976, respectively. The results of Rong et al. [100] as reported in Section 3.1 show that when u_s = 0 mm, Re_c steadily decreases, presenting the same trend with the sample G1 in Figure 12. However, for samples under shear with u_s > 0 mm, with the increment of confining pressure, Re_c firstly increases and then decreases as shown in Figure 13, presenting the same trends with most of the samples in Figure 12. For σ_n = 1.0~3.0 MPa, the range of Re_c (Re_c = 1.50~13.03) in the work of Rong et al. [100] is a little larger than that (Re_c = 0.16~9.24) of Zhou et al. [94].

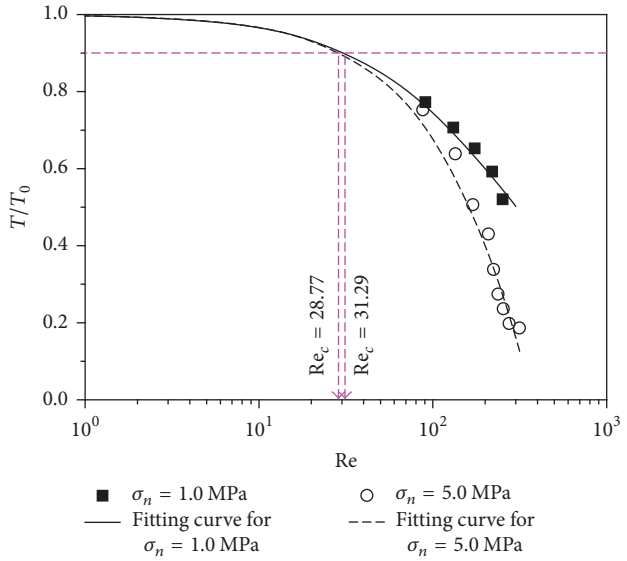

Figure 10: Relationships between T/T_0 and Re based on the data replotted from Ranjith and Darlington ([89], Figure 8).

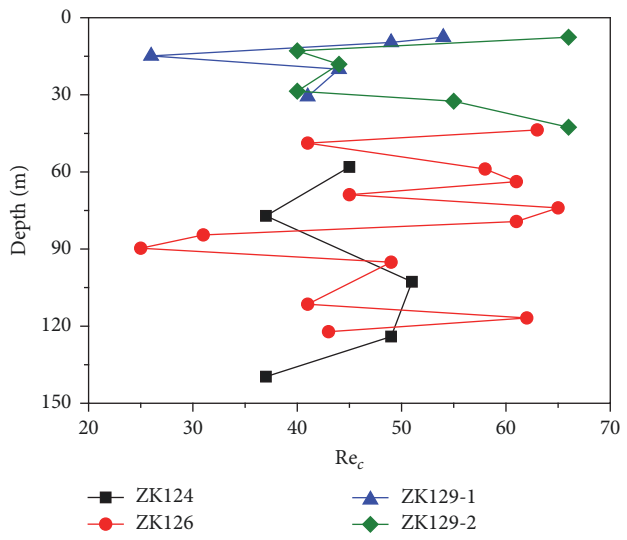

Figure 11: Relationships between depth and Re based on the data replotted from Chen et al. ([112], Tables 2–5).

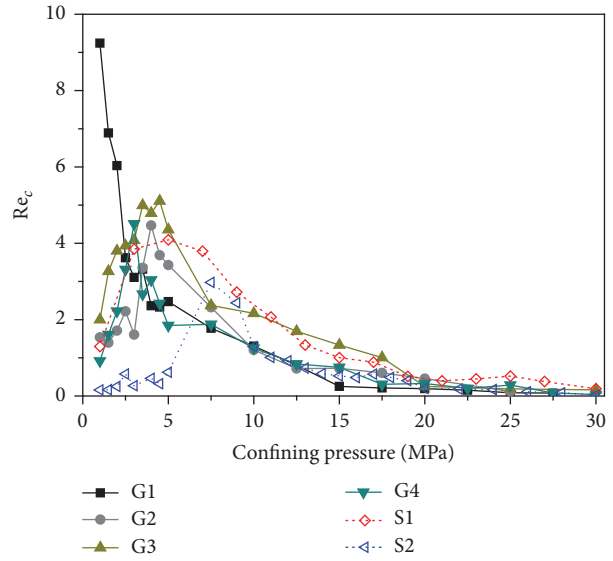

Figure 12: Relationships between Re_c and σ_n based on the data replotted from Zhou et al. ([94], Figure 8).

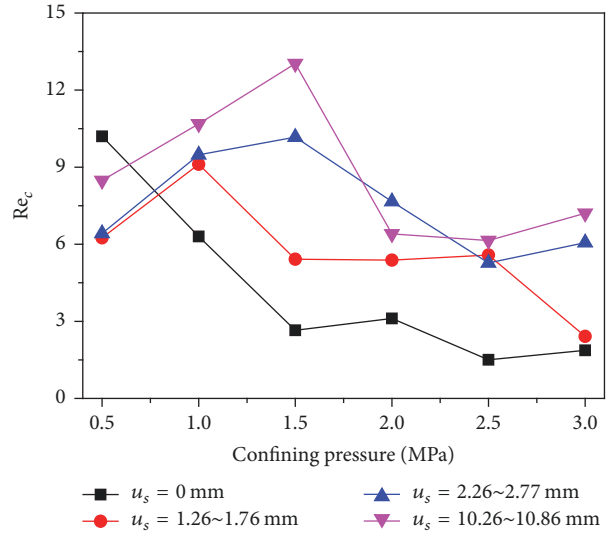

Figure 13: Relationships between Re_c and σ_n based on the data replotted from Rong et al. ([100], Figure 9).

3.3. Effect of Fracture Surface Roughness. Fracture surface roughness can alter the distributions of void spaces of fractures, especially during shear [97, 114–117]. Besides, the rougher fracture surface contributes to the longer flow paths that a particle moves within fractures, resulting in a weaker conductivity/permeability if the same pressure difference is applied on the opposing boundaries [32, 73, 118, 119]. The previous works have shown that the fracture surface roughness, especially the secondary roughness, plays a significant role on the nonlinear flow properties of rock fractures, because the eddy flow occurs due to the surface roughness [77]. Wang et al. [120] established a series of 3D self-affine rock fractures using the successive random additions (SPA) method, in which the geometry of fracture surface is fractal [121, 122]. The fractal dimension (D_3) is incorporated to characterize fracture surface roughness, which is correlated with the Hurst exponent (H) as $D_3 = 3 - H$ [123–127]. Then a 3D Lattice Boltzmann method (LBM) that has been proven to be capable of solving the NS equations [128–131] is adopted to characterize the nonlinear flow regimes in rock fractures. The results show that, with increasing fracture surface roughness represented by D_3, Re_c decreases from 47.29 to 3.78 following an exponential function (see Figure 14), because the fluid flow within the rougher fractures will enter the nonlinear flow regime from the linear regime at a lower Re. The range of Re_c (3.78~47.29) corresponding to $N_f = 0.1$ or $T/T_0 = 0.9$ is larger than that (1.8~22.0) shown in the work of Wang et al. [120],

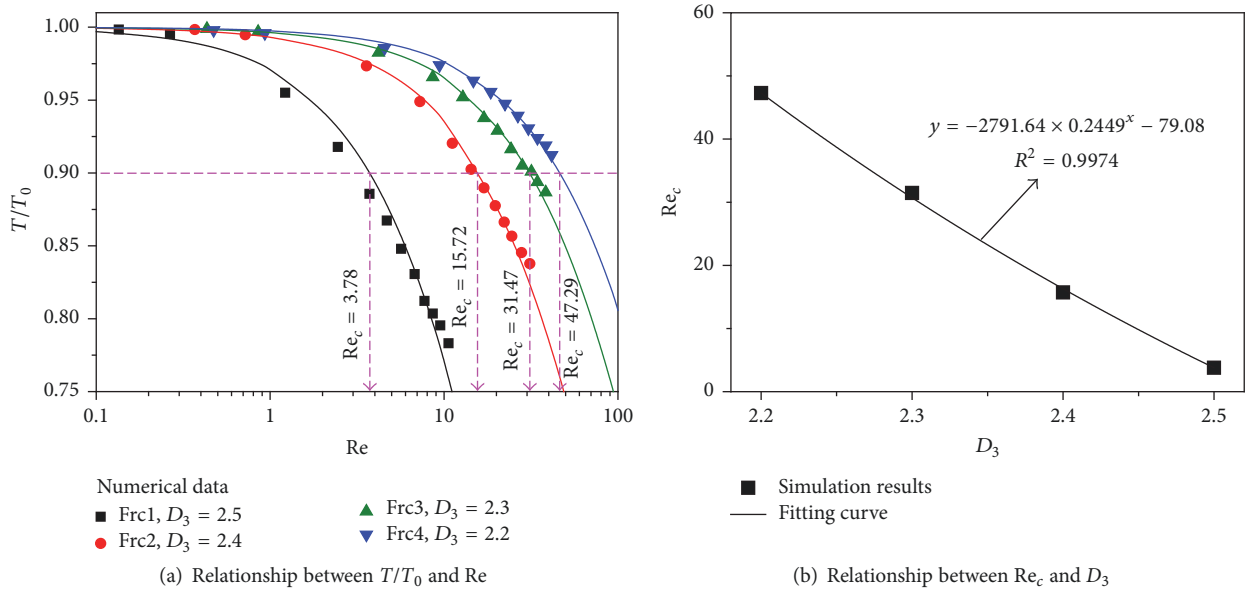

(a) Relationship between T/T_0 and Re

(b) Relationship between Re_c and D_3

FIGURE 14: Relationships between (a) T/T_0 and Re and (b) Re_c and D_3 based on the data replotted from Wang et al. ([47], Figure 16).

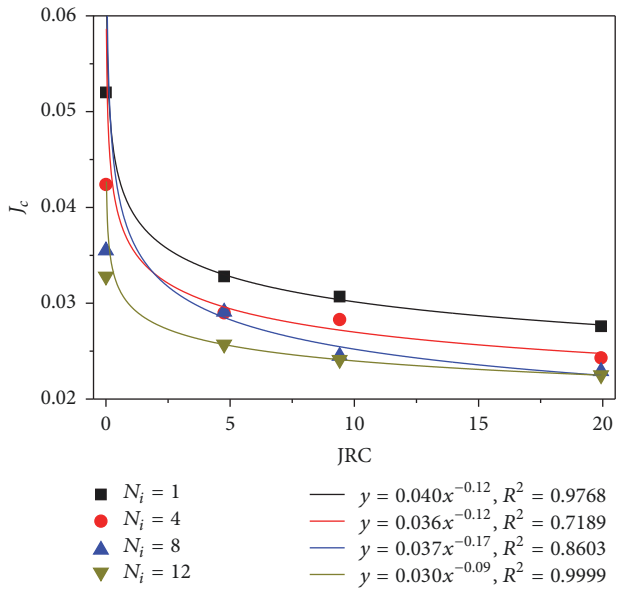

FIGURE 15: Relationships between J and Re and JRC based on the data replotted from Liu et al. ([36], Figure 6(c)).

since they utilized $N_f = 0.05$ or $T/T_0 = 0.95$ as the threshold. Liu et al. [36] studied the transition of fluid flow from the linear to the nonlinear regime and quantified the critical hydraulic gradient (J_c) for flow in simple crossed fractures and complex fracture networks. The results show that J_c decreases significantly when JRC < 5 and then decreases slightly when JRC ≥ 5, following power law functions as presented in Figure 15. Note that, in their study, the onset of nonlinear flow is categorized using $N_f = 0.01$ or $T/T_0 = 0.99$ rather than the commonly used $N_f = 0.10$ or $T/T_0 = 0.90$ due to their high-precision flow testing system that allows them to adopt a much lower critical condition. By fitting the tested and simulated results, a multivariable regression function was proposed to calculate J_c, written as

$$J_c = (\lambda E)^{-0.5} \cdot \exp\left\{300.8\,(\lambda E)^{-0.01} - 0.03\text{JRC} - 0.3N_i^{0.5} - 303.3\right\}, \quad (35)$$

where N_i is the number of intersections and λ is the coefficient that quantifies the reduction of E due to the variation of fracture apertures in a DFN.

The predicted J_c using (35) fits well with the simulation results of DFNs with well-known geometric characteristics of fractures, which verifies the validity of (35).

3.4. Effect of Fracture Aperture. In the cubic law as described in (27), flow rate is linearly proportional to the cubic of fracture aperture, indicating that fracture aperture plays a vital role in controlling fluid flow in fractures. The fracture aperture has been observed to follow lognormal distributions [132–134] and incorporated into the theoretical models [28, 135–138]. Some previous works show that fracture aperture exhibits a power law relationship with fracture length with the exponent varying from 0.5 to 2.0 [62, 139–143]. The nonlinear flow properties of fractures also depend on the magnitude of fracture aperture. Liu et al. [113] took four rock samples of granite (S1 and S2), marble (S3), and limestone (S4) from the underground caverns of the Huangdao State Oil Reserves, China, and scanned their surface geometries using a three-dimensional laser-scanning rock surface instrument [144]. A total of twenty 2D rock fractures were prepared and fracture aperture varied from 1.0 mm to 10.0 mm. Fluid flow was simulated by directly solving the NS equations, and the nonlinear flow regimes were investigated. The results show that, with the increasing J, the reduction rate of T/T_0 increases

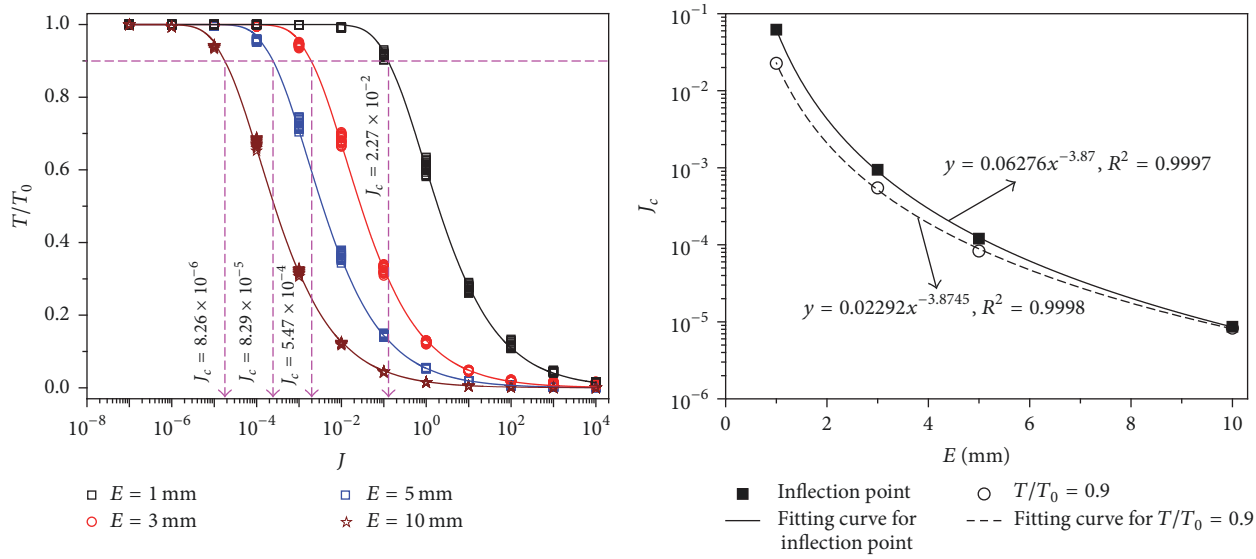

(a) Relationship between T/T_0 and J

(b) Relationship between J_c and E

FIGURE 16: Relationships between (a) T/T_0 and J and (b) J_c and E based on the data replotted from Liu et al. ([113], Figure 4).

and then decreases, existing an inflection point that has been utilized to quantify the transition from linear to nonlinear flow regime (see Figure 16(a)). With the increment of fracture aperture (E) from 1.0 mm to 10.0 mm, J_c decreases approximately four orders of magnitude following a power law function as shown in (36) and Figure 16(b).

$$J_c = 0.0627 \times E^{-3.87}. \tag{36}$$

J_c calculated corresponding to $T/T_0 = 0.9$ is smaller than that calculated corresponding to the inflection point. Based on the simple DFNs established by Liu et al. [36], the relationships between J_c and E were established as shown in Figure 17. With the increment of E from 0.5 mm to 10.0 mm, J_c decreases and spans about five orders of magnitude following power law relationships, despite the magnitude of N_i. The coefficient and exponent of the fitted equations are close to those in (36). The results show that, for both single fractures and fracture networks, J_c and E have power law correlations with a negative exponent.

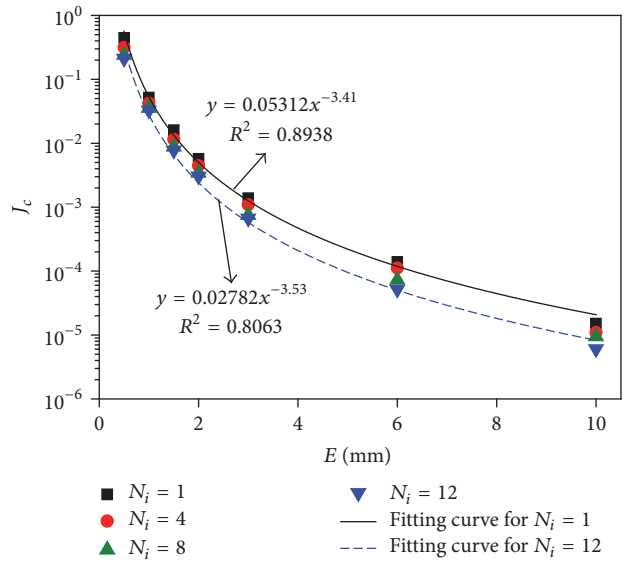

FIGURE 17: Relationships between J_c and E based on the data replotted from Liu et al. ([36], Figure 6(a)).

3.5. Effect of Fracture Intersection. Fluid is redistributed at the intersections depending on the number and geometry of fracture segments connected to the intersection [74]. Wilson and Witherspoon [145] experimentally investigated the magnitude of laminar flow interference effects at sing fracture intersections. They found that when flow is in the laminar flow regime, the inertial effects at intersections can be negligible and when Re = 100, the head loss equals about five times the pipe diameters. Kosakowski and Berkowitz [146] established numerical models with a wide variability of fracture intersection geometry and studied the streamline distributions as well as the validity of Darcy's law, by solving the NS equations using the available FEATFLOW package [147]. Their results indicate that the nonlinear inertial effects are significant for Re = 1~100, which is the range that often exists in the karst systems [14] and/or in the vicinity of wells during pump tests [15]. As introduced in the previous Sections 3.3 and 3.4, Liu et al. [36] estimated the influence of number of fracture intersections on the basis of a series of simple and complex DFNs. The results show that, with increasing N_i from 1 to 12, J_c decreases significantly and then slowly showing power law functions as shown in Figure 18. The reduction rate of J_c for JRC = 20 is about five times faster than that for JRC = 0. Comparisons among Figures 15, 17, and 18 indicate that J_c is the most sensitive to fracture aperture, followed by the number of intersections and fracture surface roughness.

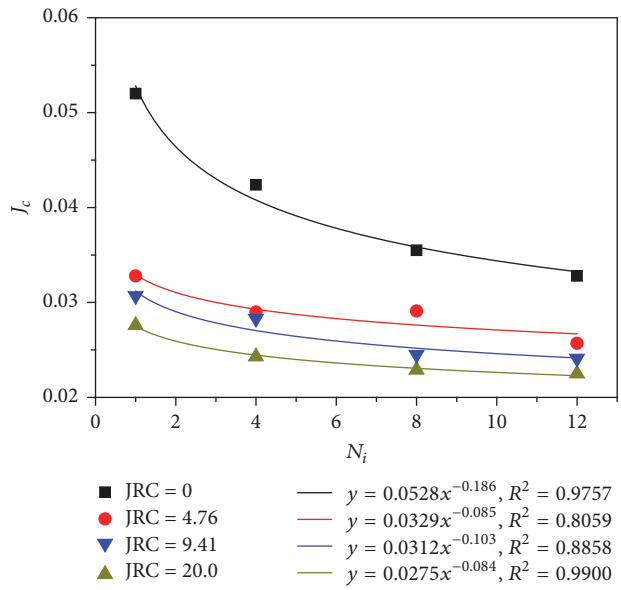

FIGURE 18: Relationships between J_c and N_i based on the data replotted from Liu et al. ([36], Figure 6(b)).

4. Conclusions

Before permeability estimation of fractured rock masses, the critical conditions for the onset of nonlinear flow such as critical Reynolds number and critical hydraulic gradient should be firstly calculated, below which the cubic law in conjunction with modifications is applicable for giving reasonable solutions and beyond which the complex Navier-Stokes equations rather than cubic law should be solved. However there exist many difficulties of solving the Navier-Stokes equations in three-dimensional single fractures and/or fracture networks, because a set of coupled nonlinear partial derivatives of varying orders should be solved and discrete fracture network models having complex geometries should be established. As a result, there are still limited works focusing on nonlinear flow properties of fluid within fractures. This is the motivation of this work that summarizes the relative works on the evolution of critical conditions for the onset of nonlinear flow and provides a reference for those who are interested in this topic.

The results show that, with the increment of shear displacement, critical Reynolds number increases significantly due to the robust effect of dilation and then increases slowly due to the weak effect of dilation. The variation trend of critical Reynolds number is close to that of fracture aperture during shear. When shear displacement varies from 0 mm to 20 mm, the critical Reynolds number increases from 0.001 to 25. The normal stress and/or confining pressure that is perpendicularly applied on the fracture would give rise to fracture aperture closure and affect the magnitude of critical Reynolds number. For most of the cases, with increasing normal stress and/or confining pressure from 0 to 30 MPa, critical Reynolds number increases firstly and then decreases, in the range 0.026~9.243. Fractures that have rougher surfaces will lose more energies due to eddy flow, resulting in the stronger nonlinear inertial effects and the smaller values of critical Reynolds number. As the fractal dimension of single three-dimensional fractures that is utilized to describe fracture surface roughness increases from 2.2 to 2.5, the critical Reynolds number decreases from 47.29 to 3.78 following an exponential function. Fracture aperture, which is a vital parameter to influence the transmissivity of fractures, plays an important role on critical hydraulic gradient. With increasing fracture aperture from 1.0 to 10.0 mm, the critical hydraulic gradient decreases for about 4~5 orders of magnitude following power law functions for both single fracture profiles and complex fracture networks. The flow paths of particles will be redistributed at fracture intersections; therefore, the fracture intersection would enhance the nonlinearity of fluid flow, resulting in a smaller critical hydraulic gradient with a larger number of intersections. The critical hydraulic gradient and number of intersections show exponential relationships. Among fracture aperture, surface roughness, and number of intersections, the critical hydraulic gradient is most sensitive to fracture aperture, followed by number of intersections and surface roughness.

Future works should be devoted on the influences of coupled (thermo-hydro-mechanical-chemical) THMC processes, precipitation-dissolution, and biogeochemistry on the evolutions of critical conditions such as critical Reynolds number and critical hydraulic gradient.

Conflicts of Interest

The authors declare that they have no conflicts of interest.

Acknowledgments

This study has been partially funded by National Basic Research 973 Program of China, China (Grant no. 2013CB036003), and National Natural Science Foundation of China, China (Grant nos. 51579239, 51323004). These supports are gratefully acknowledged.

References

[1] M. G. Gerritsen and L. J. Durlofsky, "Modeling fluid flow in oil reservoirs," *Annual Review of Fluid Mechanics*, vol. 37, pp. 211–238, 2005.

[2] C. W. MacMinn, M. L. Szulczewski, and R. Juanes, "CO_2 migration in saline aquifers. Part 1. Capillary trapping under slope and groundwater flow," *Journal of Fluid Mechanics*, vol. 662, pp. 329–351, 2010.

[3] Å. Haugen, M. A. Fernø, A. Graue, and J. Bertin H, "Experimental study of foam flow in fractured oil-wet limestone for enhanced oil recovery," *SPE Reservoir Evaluation Engineering*, vol. 15, no. 02, pp. 218–228, 2012.

[4] B. Jha and R. Juanes, "Coupled multiphase flow and poromechanics: a computational model of pore pressure effects on fault slip and earthquake triggering," *Water Resources Research*, vol. 50, no. 5, pp. 3776–3808, 2014.

[5] Y. Li, H. Zhou, W. Zhu, S. Li, and J. Liu, "Numerical investigations on slope stability using an elasto-brittle model considering

fissure water pressure," *Arabian Journal of Geosciences*, vol. 8, no. 12, pp. 10277–10288, 2015.

[6] Y. Li, H. Zhou, W. Zhu, S. Li, and J. Liu, "Numerical study on crack propagation in brittle jointed rock mass influenced by fracture water pressure," *Materials*, vol. 8, no. 6, pp. 3364–3376, 2015.

[7] P. Mora, Y. Wang, and F. Alonso-Marroquin, "Lattice solid/Boltzmann microscopic model to simulate solid/fluid systems—A tool to study creation of fluid flow networks for viable deep geothermal energy," *Journal of Earth Science*, vol. 26, no. 1, pp. 11–19, 2015.

[8] Q. Lei, J. Latham, and C. Tsang, "The use of discrete fracture networks for modelling coupled geomechanical and hydrological behaviour of fractured rocks," *Computers and Geotechnics*, vol. 85, pp. 151–176, 2017.

[9] K.-B. Min and L. Jing, "Numerical determination of the equivalent elastic compliance tensor for fractured rock masses using the distinct element method," *International Journal of Rock Mechanics and Mining Sciences*, vol. 40, no. 6, pp. 795–816, 2003.

[10] K. B. Min, J. Rutqvist, C.-F. Tsang, and L. Jing, "Stress-dependent permeability of fractured rock masses: a numerical study," *International Journal of Rock Mechanics and Mining Sciences*, vol. 41, no. 7, pp. 1191–1210, 2004.

[11] J.-Q. Zhou, S.-H. Hu, Y.-F. Chen, M. Wang, and C.-B. Zhou, "The friction factor in the forchheimer equation for rock fractures," *Rock Mechanics and Rock Engineering*, vol. 49, no. 8, pp. 3055–3068, 2016.

[12] L. Wang and B. Cardenas M, "Linear permeability evolution of expanding conduits due to feedback between flow and fast phase-change," *Geophysical Research Letters*, 2017.

[13] L. Wang and M. Bayani Cardenas, "Transition from non-Fickian to Fickian longitudinal transport through 3-D rough fractures: scale-(in)sensitivity and roughness dependence," *Journal of Contaminant Hydrology*, vol. 198, pp. 1–10, 2017.

[14] S. J. Gale, "The hydraulics of conduit flow in carbonate aquifers," *Journal of Hydrology*, vol. 70, no. 1-4, pp. 309–327, 1984.

[15] T. Kohl, K. F. Evans, R. J. Hopkirk, R. Jung, and L. Rybach, "Observation and simulation of non-Darcian flow transients in fractured rock," *Water Resources Research*, vol. 33, no. 3, pp. 407–418, 1997.

[16] Y.-F. Chen, J.-Q. Zhou, S.-H. Hu, R. Hu, and C.-B. Zhou, "Evaluation of Forchheimer equation coefficients for non-Darcy flow in deformable rough-walled fractures," *Journal of Hydrology*, vol. 529, pp. 993–1006, 2015.

[17] R. W. Zimmerman and G. S. Bodvarsson, "Hydraulic conductivity of rock fractures," *Transport in Porous Media*, vol. 23, no. 1, pp. 1–30, 1996.

[18] L. Wang, M. B. Cardenas, D. T. Slottke, R. A. Ketcham, and J. M. Sharp, "Modification of the Local Cubic Law of fracture flow for weak inertia, tortuosity, and roughness," *Water Resources Research*, vol. 51, no. 4, pp. 2064–2080, 2015.

[19] J. Cai, X. Hu, B. Xiao, Y. Zhou, and W. Wei, "Recent developments on fractal-based approaches to nanofluids and nanoparticle aggregation," *International Journal of Heat and Mass Transfer*, vol. 105, pp. 623–637, 2017.

[20] W. Zhang, B. Dai, Z. Liu, and C. Zhou, "A pore-scale numerical model for non-Darcy fluid flow through rough-walled fractures," *Computers and Geotechnics*, vol. 87, pp. 139–148, 2017.

[21] R. Liu, B. Li, Y. Jiang, and N. Huang, "Review: Mathematical expressions for estimating equivalent permeability of rock fracture networks," *Hydrogeology Journal*, vol. 24, no. 7, pp. 1623–1649, 2016.

[22] H.-H. Liu and J. Birkholzer, "On the relationship between water flux and hydraulic gradient for unsaturated and saturated clay," *Journal of Hydrology*, vol. 475, pp. 242–247, 2012.

[23] K. Develi and T. Babadagli, "Experimental and visual analysis of single-phase flow through rough fracture replicas," *International Journal of Rock Mechanics and Mining Sciences*, vol. 73, pp. 139–155, 2015.

[24] P. Davy, "On the frequency-length distribution of the San Andreas fault system," *Journal of Geophysical Research: Solid Earth*, vol. 98, no. B7, pp. 12141–12151, 1993.

[25] E. Bonnet, O. Bour, N. E. Odling et al., "Scaling of fracture systems in geological media," *Reviews of Geophysics*, vol. 39, no. 3, pp. 347–383, 2001.

[26] J.-R. De Dreuzy, P. Davy, and O. Bour, "Hydraulic properties of two-dimensional random fracture networks following a power law length distribution 1. Effective connectivity," *Water Resources Research*, vol. 37, no. 8, pp. 2065–2078, 2001.

[27] C. T. O. Leung and R. W. Zimmerman, "Estimating the Hydraulic Conductivity of Two-Dimensional Fracture Networks Using Network Geometric Properties," *Transport in Porous Media*, vol. 93, no. 3, pp. 777–797, 2012.

[28] J.-R. De Dreuzy, P. Davy, and O. Bour, "Hydraulic properties of two-dimensional random fracture networks following a power law length distribution 2. Permeability of networks based on lognormal distribution of apertures," *Water Resources Research*, vol. 37, no. 8, pp. 2079–2095, 2001.

[29] J. E. Olson, "Sublinear scaling of fracture aperture versus length: an exception or the rule?" *Journal of Geophysical Research B: Solid Earth*, vol. 108, no. 9, pp. 1–11, 2003.

[30] A. Baghbanan and L. Jing, "Hydraulic properties of fractured rock masses with correlated fracture length and aperture," *International Journal of Rock Mechanics and Mining Sciences*, vol. 44, no. 5, pp. 704–719, 2007.

[31] J.-C. Cai, B.-M. Yu, M.-Q. Zou, and M.-F. Mei, "Fractal analysis of surface roughness of particles in porous media," *Chinese Physics Letters*, vol. 27, no. 2, Article ID 024705, 2010.

[32] Z. Zhao, B. Li, and Y. Jiang, "Effects of fracture surface roughness on macroscopic fluid flow and solute transport in fracture networks," *Rock Mechanics and Rock Engineering*, pp. 1–8, 2013.

[33] R. Liu, Y. Jiang, and B. Li, "Effects of intersection and dead-end of fractures on nonlinear flow and particle transport in rock fracture networks," *Geosciences Journal*, vol. 20, no. 3, pp. 415–426, 2016.

[34] A. Zafarani and R. L. Detwiler, "An efficient time-domain approach for simulating Pe-dependent transport through fracture intersections," *Advances in Water Resources*, vol. 53, pp. 198–207, 2013.

[35] P. K. Kang, M. Dentz, T. Le Borgne, and R. Juanes, "Anomalous transport on regular fracture networks: Impact of conductivity heterogeneity and mixing at fracture intersections," *Physical Review E - Statistical, Nonlinear, and Soft Matter Physics*, vol. 92, no. 2, Article ID 022148, 2015.

[36] R. Liu, B. Li, and Y. Jiang, "Critical hydraulic gradient for nonlinear flow through rock fracture networks: The roles of aperture, surface roughness, and number of intersections," *Advances in Water Resources*, vol. 88, pp. 53–65, 2016.

[37] X. Zhang and D. J. Sanderson, "Effects of stress on the two-dimensional permeability tensor of natural fracture networks," *Geophysical Journal International*, vol. 125, no. 3, pp. 912–924, 1996.

[38] J. Rutqvist and O. Stephansson, "The role of hydromechanical coupling in fractured rock engineering," *Hydrogeology Journal*, vol. 11, no. 1, pp. 7–40, 2003.

[39] S. A. Shapiro, P. Audigane, and J.-J. Royer, "Large-scale in situ permeability tensor of rocks from induced microseismicity," *Geophysical Journal International*, vol. 137, no. 1, pp. 207–213, 1999.

[40] M. Chen, M. Bai, and J.-C. Roegiers, "Permeability tensors of anisotropic fracture networks," *Mathematical Geology*, vol. 31, no. 4, pp. 355–373, 1999.

[41] H. Auradou, G. Drazer, J. P. Hulin, and J. Koplik, "Permeability anisotropy induced by the shear displacement of rough fracture walls," *Water Resources Research*, vol. 41, no. 9, Article ID W09423, pp. 1–10, 2005.

[42] A. Baghbanan and L. Jing, "Stress effects on permeability in a fractured rock mass with correlated fracture length and aperture," *International Journal of Rock Mechanics and Mining Sciences*, vol. 45, no. 8, pp. 1320–1334, 2008.

[43] C. Clauser, "Permeability of crystalline rocks," *Eos, Transactions American Geophysical Union*, vol. 73, no. 21, pp. 233–238, 1992.

[44] C. E. Renshaw, "Sample bias and the scaling of hydraulic conductivity in fractured rock," *Geophysical Research Letters*, vol. 25, no. 1, pp. 121–124, 1998.

[45] P. Davy, O. Bour, J.-R. De Dreuzy, and C. Darcel, "Flow in multiscale fractal fracture networks," *Geological Society Special Publication*, vol. 261, pp. 31–45, 2006.

[46] Q. Wu and P. H. S. W. Kulatilake, "REV and its properties on fracture system and mechanical properties, and an orthotropic constitutive model for a jointed rock mass in a dam site in China," *Computers and Geotechnics*, vol. 43, pp. 124–142, 2012.

[47] L. Wang and M. B. Cardenas, "Development of an empirical model relating permeability and specific stiffness for rough fractures from numerical deformation experiments," *Journal of Geophysical Research: Solid Earth*, vol. 121, no. 7, pp. 4977–4989, 2016.

[48] B. Berkowitz, "Characterizing flow and transport in fractured geological media: a review," *Advances in Water Resources*, vol. 25, no. 8–12, pp. 861–884, 2002.

[49] L. Xue, H.-B. Li, E. E. Brodsky et al., "Continuous permeability measurements record healing inside the Wenchuan earthquake fault zone," *Science*, vol. 340, no. 6140, pp. 1555–1559, 2013.

[50] P. S. Lang, A. Paluszny, and R. W. Zimmerman, "Hydraulic sealing due to pressure solution contact zone growth in siliciclastic rock fractures," *Journal of Geophysical Research B: Solid Earth*, 2015.

[51] H. Yasuhara, N. Kinoshita, S. Ogata, D.-S. Cheon, and K. Kishida, "Coupled thermo-hydro-mechanical-chemical modeling by incorporating pressure solution for estimating the evolution of rock permeability," *International Journal of Rock Mechanics and Mining Sciences*, vol. 86, pp. 104–114, 2016.

[52] K. T. B. MacQuarrie and K. U. Mayer, "Reactive transport modeling in fractured rock: A state-of-the-science review," *Earth-Science Reviews*, vol. 72, no. 3-4, pp. 189–227, 2005.

[53] J. C. S. Long and P. A. Witherspoon, "Porous media equivalents for networks of discontinuous fractures," *Water Resources Research*, vol. 18, no. 3, pp. 645–658, 1982.

[54] C.-F. Tsang, "Is current hydrogeologic research addressing long-term predictions?" *Ground Water*, vol. 43, no. 3, pp. 296–300, 2005.

[55] B. Figueiredo, C.-F. Tsang, A. Niemi, and G. Lindgren, "Review: The state-of-art of sparse channel models and their applicability to performance assessment of radioactive waste repositories in fractured crystalline formations," *Hydrogeology Journal*, vol. 24, no. 7, pp. 1607–1622, 2016.

[56] J. Cai, W. Wei, X. Hu, R. Liu, and J. Wang, "Fractal characterization of dynamic fracture network extension in porous media," *Fractals*, vol. 25, no. 02, p. 1750023, 2017.

[57] I. Neretnieks, "Channeling effects in flow and transport in fractured rocks-Some recent observations and models," in *Proceedings of GEOVAL-87, International Symposium*, pp. 315–335, Stockholm, Sweden, 1987.

[58] W. S. Dershowitz and C. Fidelibus, "Derivation of equivalent pipe network analogues for three-dimensional discrete fracture networks by the boundary element method," *Water Resources Research*, vol. 35, no. 9, pp. 2685–2691, 1999.

[59] J. H. Black, J. A. Barker, and N. D. Woodman, "An investigation of sparse channel networks. Characteristic behaviours and their causes," Report R-07-35, Swedish Nuclear Fuel and Waste Management Co, Stockholm, Sweden, 2007.

[60] X. Zhang, J. D. Sanderson, M. R. Harkness, and N. C. Last, "Evaluation of the 2-D permeability tensor for fractured rock masses," *International Journal of Rock Mechanics and Mining Sciences & Geomechanics Abstracts*, vol. 33, no. 1, pp. 17–37.

[61] X. Zhang, W. Powrie, R. Harkness, and S. Wang, "Estimation of permeability for the rock mass around the shiplocks of the Three Gorges Project, China," *International Journal of Rock Mechanics and Mining Sciences*, vol. 36, no. 3, pp. 381–397, 1999.

[62] C. Klimczak, R. A. Schultz, R. Parashar, and D. M. Reeves, "Cubic law with aperture-length correlation: Implications for network scale fluid flow," *Hydrogeology Journal*, vol. 18, no. 4, pp. 851–862, 2010.

[63] Z. Zhao, L. Jing, and I. Neretnieks, "Evaluation of hydrodynamic dispersion parameters in fractured rocks," *Journal of Rock Mechanics and Geotechnical Engineering*, vol. 2, no. 3, pp. 243–254, 2010.

[64] Z. Zhao, L. Jing, I. Neretnieks, and L. Moreno, "Numerical modeling of stress effects on solute transport in fractured rocks," *Computers and Geotechnics*, vol. 38, no. 2, pp. 113–126, 2011.

[65] V. Cvetkovic, S. Painter, N. Outters, and J. O. Selroos, "Stochastic simulation of radionuclide migration in discretely fractured rock near the Äspö Hard Rock Laboratory," *Water Resources Research*, vol. 40, no. 2, 2004.

[66] Z. H. Zhao, "Gouge particle evolution in a rock fracture undergoing shear: a microscopic DEM study," *Rock Mechanics and Rock Engineering*, vol. 46, no. 6, pp. 1461–1479, 2013.

[67] R. Parashar and D. M. Reeves, "On iterative techniques for computing flow in large two-dimensional discrete fracture networks," *Journal of Computational and Applied Mathematics*, vol. 236, no. 18, pp. 4712–4724, 2012.

[68] D. M. Reeves, R. Parashar, G. Pohll, R. Carroll, T. Badger, and K. Willoughby, "The use of discrete fracture network simulations in the design of horizontal hillslope drainage networks in fractured rock," *Engineering Geology*, vol. 163, pp. 132–143, 2013.

[69] J.-P. Latham, J. Xiang, M. Belayneh, H. M. Nick, C.-F. Tsang, and M. J. Blunt, "Modelling stress-dependent permeability in fractured rock including effects of propagating and bending fractures," *International Journal of Rock Mechanics and Mining Sciences*, vol. 57, pp. 100–112, 2013.

[70] Y.-F. Chen, M.-M. Liu, S.-H. Hu, and C.-B. Zhou, "Non-Darcy's law-based analytical models for data interpretation of high-pressure packer tests in fractured rocks," *Engineering Geology*, vol. 199, pp. 91–106, 2015.

[71] D. J. Brush and N. R. Thomson, "Fluid flow in synthetic rough-walled fractures: Navier-Stokes, Stokes, and local cubic law simulations," *Water Resources Research*, vol. 39, no. 4, pp. SBH51–SBH515, 2003.

[72] M. Javadi, M. Sharifzadeh, and K. Shahriar, "A new geometrical model for non-linear fluid flow through rough fractures," *Journal of Hydrology*, vol. 389, no. 1-2, pp. 18–30, 2010.

[73] R. Liu, Y. Jiang, B. Li, and X. Wang, "A fractal model for characterizing fluid flow in fractured rock masses based on randomly distributed rock fracture networks," *Computers and Geotechnics*, vol. 65, pp. 45–55, 2015.

[74] B. Li, R. Liu, and Y. Jiang, "Influences of hydraulic gradient, surface roughness, intersecting angle, and scale effect on nonlinear flow behavior at single fracture intersections," *Journal of Hydrology*, vol. 538, pp. 440–453, 2016.

[75] A. Neuville, E. G. Flekkøy, and R. Toussaint, "Influence of asperities on fluid and thermal flow in a fracture: A coupled lattice Boltzmann study," *Journal of Geophysical Research: Solid Earth*, vol. 118, no. 7, pp. 3394–3407, 2013.

[76] L. Z. Xie, C. Gao, L. Ren, and C. B. Li, "Numerical investigation of geometrical and hydraulic properties in a single rock fracture during shear displacement with the Navier–Stokes equations," *Environmental Earth Sciences*, vol. 73, no. 11, article 28, pp. 7061–7074, 2015.

[77] L. Zou, L. Jing, and V. Cvetkovic, "Roughness decomposition and nonlinear fluid flow in a single rock fracture," *International Journal of Rock Mechanics and Mining Sciences*, vol. 75, pp. 102–118, 2015.

[78] R. Temam, *Navier-Stokes Equations*, North-Holland Publishing, Amsterdam, The Netherlands, 1984.

[79] S. H. Lee, K.-K. Lee, and I. W. Yeo, "Assessment of the validity of Stokes and Reynolds equations for fluid flow through a rough-walled fracture with flow imaging," *Geophysical Research Letters*, vol. 41, no. 13, pp. 4578–4585, 2014.

[80] J. B. Bell, J. A. Trangenstein, and G. . Shubin, "Conservation laws of mixed type describing three-phase flow in porous media," *SIAM Journal on Applied Mathematics*, vol. 46, no. 6, pp. 1000–1017, 1986.

[81] C. Xia, X. Qian, P. Lin, W. Xiao, and Y. Gui, "Experimental investigation of nonlinear flow characteristics of real rock joints under different contact conditions," *Journal of Hydraulic Engineering*, vol. 143, no. 3, p. 04016090, 2017.

[82] P. Forchheimer, "Wasserbewegung durch Boden," *Zeitschrift des Vereines Deutscher Ingenieure*, vol. 45, pp. 1782–1788, 1901.

[83] J. Bear, *Dynamics of Fluids in Porous Media*, American Elsevier, New York, NY, USA, 1972.

[84] K. N. Moutsopoulos, "Exact and approximate analytical solutions for unsteady fully developed turbulent flow in porous media and fractures for time dependent boundary conditions," *Journal of Hydrology*, vol. 369, no. 1-2, pp. 78–89, 2009.

[85] J. Qian, H. Zhan, Z. Chen, and H. Ye, "Experimental study of solute transport under non-Darcian flow in a single fracture," *Journal of Hydrology*, vol. 399, no. 3-4, pp. 246–254, 2011.

[86] C. Cherubini, C. I. Giasi, and N. Pastore, "Bench scale laboratory tests to analyze non-linear flow in fractured media," *Hydrology and Earth System Sciences*, vol. 16, no. 8, pp. 2511–2522, 2012.

[87] P. M. Adler, A. E. Malevich, and V. V. Mityushev, "Nonlinear correction to Darcy's law for channels with wavy walls," *Acta Mechanica*, vol. 224, no. 8, pp. 1823–1848, 2013.

[88] R. W. Zimmerman, A. Al-Yaarubi, C. C. Pain, and C. A. Grattoni, "Non-linear regimes of fluid flow in rock fractures," *International Journal of Rock Mechanics and Mining Sciences*, vol. 41, no. 1, pp. 1–7, 2004.

[89] P. G. Ranjith and W. Darlington, "Nonlinear single-phase flow in real rock joints," *Water Resources Research*, vol. 43, no. 9, Article ID W09502, 2007.

[90] M. Javadi, M. Sharifzadeh, K. Shahriar, and Y. Mitani, "Critical Reynolds number for nonlinear flow through rough-walled fractures: the role of shear processes," *Water Resources Research*, vol. 50, no. 2, pp. 1789–1804, 2014.

[91] E. Skjetne, A. Hansen, and J. S. Gudmundsson, "High-velocity flow in a rough fracture," *Journal of Fluid Mechanics*, vol. 383, pp. 1–28, 1999.

[92] Z. Zeng and R. Grigg, "A criterion for non-darcy flow in porous media," *Transport in Porous Media*, vol. 63, no. 1, pp. 57–69, 2006.

[93] G. Rong, D. Hou, J. Yang, L. Cheng, and C. Zhou, "Experimental study of flow characteristics in non-mated rock fractures considering 3D definition of fracture surfaces," *Engineering Geology*, vol. 220, pp. 152–163, 2017.

[94] J.-Q. Zhou, S.-H. Hu, S. Fang, Y.-F. Chen, and C.-B. Zhou, "Nonlinear flow behavior at low Reynolds numbers through rough-walled fractures subjected to normal compressive loading," *International Journal of Rock Mechanics and Mining Sciences*, vol. 80, pp. 202–218, 2015.

[95] X. Xiong, B. Li, Y. Jiang, T. Koyama, and C. Zhang, "Experimental and numerical study of the geometrical and hydraulic characteristics of a single rock fracture during shear," *International Journal of Rock Mechanics and Mining Sciences*, vol. 48, no. 8, pp. 1292–1302, 2011.

[96] I. W. Yeo, M. H. De Freitas, and R. W. Zimmerman, "Effect of shear displacement on the aperture and permeability of a rock fracture," *International Journal of Rock Mechanics and Mining Sciences*, vol. 35, no. 8, pp. 1051–1070, 1998.

[97] R. Olsson and N. Barton, "An improved model for hydromechanical coupling during shearing of rock joints," *International Journal of Rock Mechanics and Mining Sciences*, vol. 38, no. 3, pp. 317–329, 2001.

[98] H. S. Lee and T. F. Cho, "Hydraulic characteristics of rough fractures in linear flow under normal and shear load," *Rock Mechanics and Rock Engineering*, vol. 35, no. 4, pp. 299–318, 2002.

[99] T. Koyama, N. Fardin, L. Jing, and O. Stephansson, "Numerical simulation of shear-induced flow anisotropy and scale-dependent aperture and transmissivity evolution of rock fracture replicas," *International Journal of Rock Mechanics and Mining Sciences*, vol. 43, no. 1, pp. 89–106, 2006.

[100] G. Rong, J. Yang, L. Cheng, and C. B. Zhou, "Laboratory investigation of nonlinear flow characteristics in rough fractures during shear process," *Journal of Hydrology*, vol. 541, pp. 1385–1394, 2016.

[101] I. W. Yao, *Anisotropic hydraulic properties of a rock fracture under normal and shear loading [Ph.D. thesis]*, London, UK, Imperial College, 1998.

[102] A. Al-Yaarubi, *Numerical and experimental study of fluid flow in a rough-walled rock fracture [Ph.D. thesis]*, London, UK, Imperial College, 2003.

[103] C. Louis, *Rock Hydraulics in Rock Mechanics*, Springer-New Verlag, New York, NY, USA, 1974.

[104] C. R. McKee, A. C. Bumb, and R. A. Koenig, "Stress-dependent permeability and porosity of coal and other geologic formations," *SPE Formation Evaluation*, vol. 3, no. 1, pp. 81–91, 1988.

[105] W. B. Durham, "Laboratory observations of the hydraulic behavior of a permeable fracture from 3800 m depth in the KTB pilot hole," *Journal of Geophysical Research B: Solid Earth*, vol. 102, no. 8, pp. 18405–18416, 1997.

[106] G. R. L. Chalmers, D. J. K. Ross, and R. M. Bustin, "Geological controls on matrix permeability of Devonian Gas Shales in the Horn River and Liard basins, northeastern British Columbia, Canada," *International Journal of Coal Geology*, vol. 103, pp. 120–131, 2012.

[107] Y. Cho, O. G. Apaydin, and E. Ozkan, "Pressure-dependent natural-fracture permeability in shale and its effect on shale-gas well production," *SPE Reservoir Evaluation and Engineering*, vol. 16, no. 2, pp. 216–228, 2013.

[108] D. Chen, Z. Pan, and Z. Ye, "Dependence of gas shale fracture permeability on effective stress and reservoir pressure: Model match and insights," *Fuel*, vol. 139, pp. 383–392, 2015.

[109] S. C. Bandis, A. C. Lumsden, and N. R. Barton, "Fundamentals of rock joint deformation," *International Journal of Rock Mechanics and Mining Sciences & Geomechanics Abstracts*, vol. 20, no. 6, pp. 249–268, 1983.

[110] B. Li, Z. Zhao, Y. Jiang, and L. Jing, "Contact mechanism of a rock fracture subjected to normal loading and its impact on fast closure behavior during initial stage of fluid flow experiment," *International Journal for Numerical and Analytical Methods in Geomechanics*, vol. 39, no. 13, pp. 1431–1449, 2015.

[111] Z. Zhang and J. Nemcik, "Fluid flow regimes and nonlinear flow characteristics in deformable rock fractures," *Journal of Hydrology*, vol. 477, pp. 139–151, 2013.

[112] Y.-F. Chen, S.-H. Hu, R. Hu, and C.-B. Zhou, "Estimating hydraulic conductivity of fractured rocks from high-pressure packer tests with an Izbash's law-based empirical model," *Water Resources Research*, vol. 51, no. 4, pp. 2096–2118, 2015.

[113] R. Liu, L. Yu, and Y. Jiang, "Quantitative estimates of normalized transmissivity and the onset of nonlinear fluid flow through rough rock fractures," *Rock Mechanics and Rock Engineering*, vol. 50, no. 4, pp. 1063–1071, 2017.

[114] Y. Méheust and J. Schmittbuhl, "Flow enhancement of a rough fracture," *Geophysical Research Letters*, vol. 27, no. 18, pp. 2989–2992, 2000.

[115] I. W. Yeo, "Effect of contact obstacles on fluid flow in rock fractures," *Geosciences Journal*, vol. 5, no. 2, pp. 139–143, 2001.

[116] J. Kim, W. Cho, I.-M. Chung, and J.-H. Heo, "On the stochastic simulation procedure of estimating critical hydraulic gradient for gas storage in unlined rock caverns," *Geosciences Journal*, vol. 11, no. 3, pp. 249–258, 2007.

[117] K. Matsuki, Y. Kimura, K. Sakaguchi, A. Kizaki, and A. A. Giwelli, "Effect of shear displacement on the hydraulic conductivity of a fracture," *International Journal of Rock Mechanics and Mining Sciences*, vol. 47, no. 3, pp. 436–449, 2010.

[118] S. Luo, Z. Zhao, H. Peng, and H. Pu, "The role of fracture surface roughness in macroscopic fluid flow and heat transfer in fractured rocks," *International Journal of Rock Mechanics and Mining Sciences*, vol. 87, pp. 29–38, 2016.

[119] Y. He, B. Bai, S. Hu, and X. Li, "Effects of surface roughness on the heat transfer characteristics of water flow through a single granite fracture," *Computers and Geotechnics*, vol. 80, pp. 312–321, 2016.

[120] M. Wang, Y.-F. Chen, G.-W. Ma, J.-Q. Zhou, and C.-B. Zhou, "Influence of surface roughness on nonlinear flow behaviors in 3D self-affine rough fractures: Lattice Boltzmann simulations," *Advances in Water Resources*, vol. 96, pp. 373–388, 2016.

[121] H.-H. Liu, G. S. Bodvarsson, S. Lu, and F. J. Molz, "A corrected and generalized successive random additions algorithm for simulating fractional levy motions," *Mathematical Geology*, vol. 36, no. 3, pp. 361–378, 2004.

[122] Z. Ye, H.-H. Liu, Q. Jiang, and C. Zhou, "Two-phase flow properties of a horizontal fracture: The effect of aperture distribution," *Advances in Water Resources*, vol. 76, pp. 43–54, 2015.

[123] B. B. Mandelbrot, *The Fractal Geometry of Nature*, Henry Holt and Company, San Francisco, Calif, USA, 1983.

[124] S. R. Brown and C. H. Scholz, "Broad bandwidth study of the topography of natural rock surfaces," *Journal of Geophysical Research*, vol. 90, no. B14, p. 12575, 1985.

[125] N. E. Odling, "Natural fracture profiles, fractal dimension and joint roughness coefficients," *Rock Mechanics and Rock Engineering*, vol. 27, no. 3, pp. 135–153, 1994.

[126] R. Liu, L. Yu, and Y. Jiang, "Fractal analysis of directional permeability of gas shale fracture networks: a numerical study," *Journal of Natural Gas Science and Engineering*, vol. 33, pp. 1330–1341, 2016.

[127] B. Li, R. Liu, and Y. Jiang, "A multiple fractal model for estimating permeability of dual-porosity media," *Journal of Hydrology*, vol. 540, pp. 659–669, 2016.

[128] R. Benzi, S. Succi, and M. Vergassola, "The lattice Boltzmann equation: theory and applications," *Physics Reports*, vol. 222, no. 3, pp. 145–197, 1992.

[129] Y. H. Qian, D. D'Humières, and P. Lallemand, "Lattice BGK models for Navier-Stokes equation," *EPL (Europhysics Letters)*, vol. 17, no. 6, p. 479, 1992.

[130] S. Succi, *The Lattice Boltzmann Equation for Fluid Dynamics and Beyond*, Oxford University Press, Oxford, UK, 2001.

[131] D. A. Wolf-Gladrow, *Lattice-Gas Cellular Automata and Lattice Boltzmann Models: An Introduction*, Springer, 2004.

[132] B. Dverstorp and J. Andersson, "Application of the discrete fracture network concept with field data: possibilities of model calibration and validation," *Water Resources Research*, vol. 25, no. 3, pp. 540–550, 1989.

[133] M. C. Cacas, E. Ledoux, G. de Marsily et al., "Modeling fracture flow with a stochastic discrete fracture network: calibration and validation: 1. The flow model," *Water Resources Research*, vol. 26, no. 3, pp. 479–489, 1990.

[134] J. H. Li and L. M. Zhang, "Geometric parameters and REV of a crack network in soil," *Computers and Geotechnics*, vol. 37, no. 4, pp. 466–475, 2010.

[135] J. C. S. Long and D. M. Billaux, "From field data to fracture network modeling: An example incorporating spatial structure," *Water Resources Research*, vol. 23, no. 7, pp. 1201–1216, 1987.

[136] E. Charlaix, E. Guyon, and S. Roux, "Permeability of a random array of fractures of widely varying apertures," *Transport in Porous Media*, vol. 2, no. 1, pp. 31–43, 1987.

[137] G. Margolin, B. Berkowitz, and H. Scher, "Structure, flow, and generalized conductivity scaling in fracture networks," *Water Resources Research*, vol. 34, no. 9, pp. 2103–2121, 1998.

[138] J.-R. De Dreuzy, P. Davy, and O. Bour, "Hydraulic properties of two-dimensional random fracture networks following power law distributions of length and aperture," *Water Resources Research*, vol. 38, no. 12, pp. 121–129, 2002.

[139] J. J. Walsh and J. Watterson, "Analysis of the relationship between displacements and dimensions of faults," *Journal of Structural Geology*, vol. 10, no. 3, pp. 239–247, 1988.

[140] P. A. Gillespie, J. J. Walsh, and J. Watterson, "Limitations of dimension and displacement data from single faults and the consequences for data analysis and interpretation," *Journal of Structural Geology*, vol. 14, no. 10, pp. 1157–1172, 1992.

[141] H. Fossen and J. Hesthammer, "Geometric analysis and scaling relations of deformation bands in porous sandstone," *Journal of Structural Geology*, vol. 19, no. 12, pp. 1479–1493, 1997.

[142] C. H. Scholz, *The Mechanics of Earthquakes and Faulting*, Cambridge University Press, Cambridge, UK, 2002.

[143] R. A. Schultz, R. Soliva, H. Fossen, C. H. Okubo, and D. M. Reeves, "Dependence of displacement-length scaling relations for fractures and deformation bands on the volumetric changes across them," *Journal of Structural Geology*, vol. 30, no. 11, pp. 1405–1411, 2008.

[144] G. Wang, X. Zhang, Y. Jiang, X. Wu, and S. Wang, "Rate-dependent mechanical behavior of rough rock joints," *International Journal of Rock Mechanics and Mining Sciences*, vol. 83, pp. 231–240, 2016.

[145] C. R. Wilson and P. A. Witherspoon, "Flow interference effects at fracture intersections," *Water Resources Research*, vol. 12, no. 1, pp. 102–104, 1976.

[146] G. Kosakowski and B. Berkowitz, "Flow pattern variability in natural fracture intersections," *Geophysical Research Letters*, vol. 26, no. 12, pp. 1765–1768, 1999.

[147] S. Turek, *Efficient Solvers for Incompressible Flow Problems: An Algorithmic and Computational Approach*, Springer Science & Business Media, 1999.